The GTPase Rab27b regulates the release, autophagic clearance, and toxicity of α-synuclein

Received for publication, March 9, 2020, and in revised form, April 24, 2020 Published, Papers in Press, April 29, 2020, DOI 10.1074/jbc.RA120.013337

Rachel Underwood[1], Bing Wang[1], Christine Carico[2], Robert H. Whitaker[2], William J. Placzek[2], and Talene A. Yacoubian[1,*]

From the [1]Center for Neurodegeneration and Experimental Therapeutics, Department of Neurology and the [2]Department of Biochemistry and Molecular Genetics, University of Alabama at Birmingham, Birmingham, Alabama

Edited by Paul E. Fraser

α-Synuclein (αsyn) is the primary component of proteinaceous aggregates termed Lewy bodies that pathologically define synucleinopathies including Parkinson's disease (PD) and dementia with Lewy bodies (DLB). αsyn is hypothesized to spread through the brain in a prion-like fashion by misfolded protein forming a template for aggregation of endogenous αsyn. The cell-to-cell release and uptake of αsyn are considered important processes for its prion-like spread. Rab27b is one of several GTPases essential to the endosomal-lysosomal pathway and is implicated in protein secretion and clearance, but its role in αsyn spread has yet to be characterized. In this study, we used a paracrine αsyn *in vitro* neuronal model to test the impact of Rab27b on αsyn release, clearance, and toxicity. shRNA-mediated knockdown (KD) of Rab27b increased αsyn-mediated paracrine toxicity. Rab27b reduced αsyn release primarily through nonexosomal pathways, but the αsyn released after Rab27b KD was of higher-molecular-weight species, as determined by size-exclusion chromatography. Rab27b KD increased intracellular levels of insoluble αsyn and led to an accumulation of endogenous light chain 3 (LC3)-positive puncta. Rab27b KD also decreased LC3 turnover after treatment with an autophagosome-lysosome fusion inhibitor, chloroquine, indicating that Rab27b KD induces a defect in autophagic flux. Rab27b protein levels were increased in brain lysates obtained from postmortem tissues of individuals with PD and DLB compared with healthy controls. These data indicate a role for Rab27b in the release, clearance, and toxicity of αsyn and, ultimately, in the pathogenesis of synucleinopathies.

Synucleinopathies, such as Parkinson's disease (PD) and dementia with Lewy bodies (DLB), have tremendous economic and social impact, yet there are no current therapies to slow neurodegeneration in PD or DLB (1). α-Synuclein (αsyn) is the key pathogenic protein implicated in both PD and DLB. Recent evidence suggests that misfolded αsyn propagates from neuron to neuron in a prion-like manner: transmission of misfolded αsyn templates misfolding of endogenous αsyn to promote further aggregation and ultimately neurotoxicity (2–4). Propagation of αsyn requires three distinct cellular processes: release, uptake, and misfolding. αsyn does not have a signal peptide and is not released via the classic endoplasmic reticulum–Golgi secretory pathway (5, 6). There is evidence that αsyn is released through nonclassical endosomal pathways, including exosomal, misfolding-associated protein secretion, and lysosomal pathways (7–13). These pathways are thought to be tightly regulated by the Rab family of GTPase proteins.

Rab GTPases are a largely conserved family of proteins with over 60 known mammalian members. Rab proteins' primary functions are carried out through a catalytic GTP/GDP binding site, which, when GTP-bound, causes a conformational switch allowing the protein to interact with its effector proteins and thus regulate multiple cellular processes (14). Several Rab GTPases have been associated with PD. Mutations in Rab39b and Rab32 cause autosomal recessive forms of early-onset and late-onset PD, respectively (15–17). Rabs regulate autophagic, exocytotic, and endocytotic pathways potentially involved in αsyn transmission. A number of Rab GTPases regulate αsyn trafficking (18). Overexpression of Rab1, -7, -8, or -11 is protective against αsyn toxicity, and these Rabs are implicated in αsyn aggregate formation in PD models (19–24). Additionally, Rabs have been shown to be kinase substrates of LRRK2, mutations of which are the most common genetic cause of PD (25).

Rab27b is a relatively unstudied member of the Rab GTPase family. Pointing to a potential functional overlap between the two proteins, Rab27b shares common regulators and effectors with Rab3, which binds αsyn and is localized in αsyn aggregates (14, 22, 26–28). Rab27b can regulate protein secretion through both exosomal and nonexosomal pathways by regulating transport and docking steps in tandem with Rab27a through interaction with several Rab27 effectors (29–35). Rab27b and its effectors regulate exocytosis of dense-core vesicles in neuronal lines and synaptic vesicle release in neurons (27, 28, 36–38). Unlike Rab27a, Rab27b is highly expressed in neurons in the cortex, striatum, and midbrain, areas affected in PD and DLB (29, 39).

Rab27b may also play a role in protein clearance via autophagy. Rab27b is localized to the autophagosome under stress conditions that induce autophagy (40). Rab27a/b double knockout mice show increased vesicle formation, including lysosomes and autophagosomes, in the lacrimal gland (41). Evidence for autophagic-lysosomal pathway impairment in PD is growing (42–46). The presence of Rab27b in the autophagic-lysosomal process indicates the potential for Rab27b to alter not only αsyn release but αsyn clearance as well.

This article contains supporting information.

* For correspondence: Talene A. Yacoubian, tyacoubian@uabmc.edu.

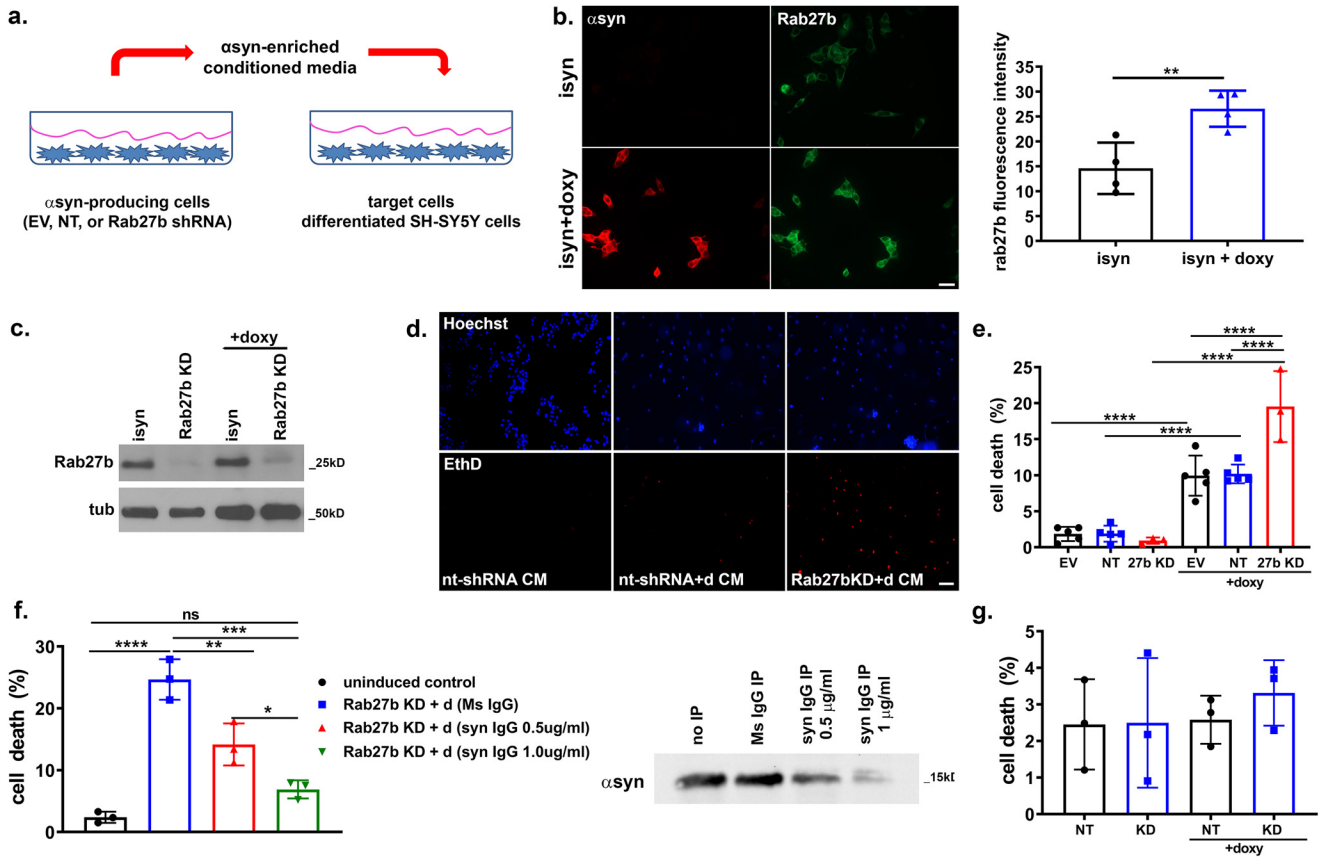

Figure 1. Rab27b knockdown in isyn cells increases αsyn-induced paracrine toxicity. *a*, schematic of αsyn paracrine toxicity model. isyn cells transfected with plko.1 EV, nt-shRNA (*NT*), or Rab27b shRNA overexpress and release αsyn into CM when treated with doxy. Cell death is induced in recipient cells treated with αsyn-enriched CM. *b*, Rab27b immunoreactivity increased in isyn cells upon αsyn overexpression. Shown are representative images of Rab27b (*green*) and αsyn (*red*) immunoreactivity in uninduced isyn cells and in isyn cells when induced with doxy for 48 h. *Scale bar*, 25 μm. $n = 4$; Student's *t* test: $t_6 = 3.793$; **, $p \leq 0.01$. *c*, Rab27b KD by shRNA reduces Rab27b protein levels in both uninduced and induced isyn cells. *d*, Rab27b KD increases αsyn-induced paracrine toxicity in differentiated SH-SY5Y cells treated with CM. Shown are representative images of differentiated SH-SY5Y cells treated with CM from isyn cells or isyn cells transduced with nt-shRNA or Rab27b shRNA. Ethidium D labels the nuclei of dying cells, whereas Hoechst 33342 stains the nuclei of all cells. *Scale bar*, 50 μm. *e*, quantification of cell death in differentiated SH-SY5Y cells treated with CM from isyn cells transduced with EV, nt-shRNA, or Rab27b shRNA for 48 h. $n = 3$ independent rounds with 1–2 replicates/round. One-way ANOVA: $F_{(3, 8)} = 44.90$, $p \leq 0.0001$. Tukey's multiple-comparison test: ****, $p \leq 0.0001$. *f*, immunoprecipitation of αsyn from CM by αsyn-directed mAb reduces the toxicity of αsyn-enriched CM from isyn/Rab27b KD cells in a dose-dependent manner. Shown is quantification of cell death in differentiated SH-SH5Y cells treated with CM from induced isyn/Rab27b KD cells in which αsyn was immunodepleted. Western blotting of CM after immunoprecipitation confirms reduction of αsyn in the CM. $n = 3$ independent rounds with 1 replicate/round. One-way ANOVA: $F_{(5, 20)} = 39.10$, $p \leq 0.0001$. Tukey's multiple comparison test: *, $p \leq 0.05$; **, $p \leq 0.01$; ***, $p \leq 0.001$; ****, $p \leq 0.0001$; *ns*, nonsignificant. *g*, Rab27b KD does not induce cell death in isyn cells. Shown is quantification of cell death in isyn transduced with nt-shRNA or Rab27b shRNA with and without doxy induction. The number of ethidium D–positive cells is normalized to total cell count, as determined by Hoechst 33342 staining. $n = 3$ independent rounds with 1 replicate/round. One-way ANOVA: $F_{(3, 8)} = 0.3343$, $p > 0.05$. *Error bars*, S.D. *D*, doxy.

Rab27b has been linked to several neurodegenerative disorders. Elevated Rab27b expression in cholinergic basal forebrain neurons is associated with cognitive decline in mild cognitive impairment and Alzheimer's disease (47). In addition, multiple Rab27b polymorphisms have been associated with a higher risk for motor neuron disease in GWAS studies (48). Alterations in Rab27b expression are observed in a cellular model for X-linked dystonia parkinsonism syndrome and in human DLB brains (49, 50).

Because of its function in regulating protein secretion and autophagy, we hypothesized that Rab27b regulates cell-to-cell transmission of αsyn by regulation of αsyn release and clearance. Here, we examine the effect of Rab27b on αsyn toxicity in an *in vitro* paracrine αsyn model and evaluate the impact of Rab27b on αsyn release and clearance via autophagy. We found that Rab27b reduces αsyn toxicity by promoting autophagic flux.

Results

Rab27b reduces αsyn-induced paracrine toxicity

We have developed a paracrine αsyn model using a doxycycline (doxy)-inducible neuroblastoma cell line, termed isyn, to evaluate the toxicity associated with neuronally released αsyn (Fig. 1*a*) (51). We have previously shown that induction of αsyn expression with doxy in isyn cells leads to the detection of αsyn in the CM in a dose-dependent manner and that fractionation of the CM into exosomal and nonexosomal fractions by sequential, high-ultracentrifugation techniques shows that αsyn is released into both exosomal and nonexosomal fractions (51). Additionally, we have previously established that released αsyn is toxic to separately cultured neurons: transfer of αsyn-enriched CM from induced isyn cells promotes cell death of separately cultured differentiated SH-SY5Y neuroblastoma cells or primary mouse neurons (51). Toxicity from αsyn-en-

riched CM depends on αsyn, as immunodepletion of αsyn from the CM eliminated toxicity in a dose-dependent manner (51). An initial PCR screen for detectable expression of potential exosome-related proteins in isyn cells pointed to Rab27b and Rab35 expression in isyn cells. Upon αsyn induction with doxy (10 μg/ml), Rab27b expression increased by nearly 2-fold, as determined by immunocytochemistry (Fig. 1*b*). We confirmed the increase in Rab27b by Western blotting (Fig. S1). No change was noted in Rab35 expression (Fig. S2*a*).

Given the increase in Rab27b expression upon αsyn induction in isyn cells, we tested whether Rab27b knockdown (KD) could affect the toxicity of released αsyn. isyn cells were transduced with Rab27b targeted shRNA lentivirus selectable by puromycin. Rab27b KD in isyn cells was confirmed by Western blotting (Fig. 1*c*). As controls for Rab27b KD, isyn cells were transduced with either plko.1 empty vector (EV) lentivirus or with nontarget shRNA (nt-shRNA) lentivirus. Toxicity of αsyn-enriched CM was increased with Rab27b KD upon doxy induction in isyn cells compared with both isyn controls. Separately cultured differentiated SH-SY5Y showed ~10% cell death at 24 h when treated with CM from induced control isyn cells, but toxicity was doubled when treated with CM from induced isyn cells with Rab27b KD (Fig. 1, *d* and *e*). Increased toxicity from αsyn-enriched medium from Rab27b KD/isyn cells depended on αsyn, as immunodepletion of αsyn from the CM eliminated toxicity in a dose-dependent manner (Fig. 1*f*). Rab27b KD did not impact cell death at baseline in isyn cells (Fig. 1*g*).

Rab27b regulates αsyn release

Rab27b regulates protein secretion through both exosomal and nonexosomal pathways (29–35). As Rab27b KD increased the toxicity of αsyn released by isyn cells, we next examined whether Rab27b regulated the amount of αsyn released in this paracrine model system. Surprisingly, upon doxy induction, we observed a nearly 60% decrease in the total amount of αsyn released into the CM in isyn cells with Rab27b KD compared with control isyn cells transduced with nt-shRNA (Fig. 2). Differences in release were not due to cell death, as cell death was limited to ~2–4% in induced isyn cells with and without Rab27b KD (Fig. 1*g*). These data indicate that the increase in αsyn toxicity with Rab27b KD was not due to a total increase in αsyn release.

Previous research has shown that αsyn is released through exosomal and nonexosomal pathways, and certain studies have suggested that exosomally released αsyn may have increased toxic potential (5, 10, 11, 52). We fractionated the CM into exosomal and nonexosomal fractions by sequential, high-ultracentrifugation techniques (53) to test whether Rab27b KD possibly preferentially inhibited release through nonexosomal pathways. The vast majority of released αsyn in our model is associated with the nonexosomal fraction from isyn cells (51). When Rab27b was knocked down in isyn cells, the amount of αsyn released in the nonexosomal fraction was decreased by 44% compared with nt-shRNA control (Fig. 2*e*). The amount of αsyn released in the exosomal fraction was also decreased relative to control isyn cells (Fig. 2*f*). NanoSight analysis confirmed nanometer-sized vesicle sizes consistent with exosomes released into the CM (51) (Fig. 2*b*). Thus, the total change in αsyn release induced by Rab27b KD occurred through nonexosomal and exosomal pathways.

Rab27b promotes autophagic flux and αsyn clearance

Our previous work in the paracrine αsyn model revealed that the type of αsyn species released was the critical factor that mediates toxicity, not the total amount of αsyn released (51). This finding suggests that oligomeric, toxic αsyn species are potentially available for release. To biochemically characterize αsyn released into the CM, we used size-exclusion chromatography (SEC). We and others have previously shown that much of the released αsyn is found in higher-molecular-weight fractions representing molecular sizes greater than 14 kDa, the expected monomeric αsyn size by SEC (5, 51, 54). We fractionated CM from induced nt-shRNA/isyn cells and induced isyn/Rab27b KD cells by SEC and found that the amount of released αsyn released into higher-molecular-weight fractions was significantly increased by Rab27b KD (Fig. 3, *a* and *b*). ELISA of total CM prior to SEC fractionation confirmed that total αsyn levels was overall lower in the CM from isyn cells with Rab27b KD compared with that from induced nt-shRNA isyn cells despite the increase in higher molecular weight αsyn (Fig. S3).

Given the increase in high-molecular weight αsyn species released in the presence of Rab27b KD, we hypothesized that Rab27b promotes the clearance of intracellular αsyn. We next examined whether insoluble αsyn levels were altered in induced isyn cells upon Rab27b KD. Whereas αsyn levels in the Triton X-100 soluble fraction did not statistically differ, we observed more αsyn in the Triton X-100–insoluble fraction in isyn cells with Rab27b KD (Fig. 3*c*).

Misfolded proteins are typically cleared through the autophagic pathway or through the proteasome. αsyn, particularly oligomeric species, has been previously shown to be degraded through autophagy (46, 55). We hypothesized that Rab27b promotes αsyn clearance via the autophagic-lysosomal pathway. We first examined levels of proteins involved in the endosomal-lysosomal system in doxy-induced isyn with and without Rab27b KD cells under serum starvation. Rab7, a late endosome marker, and p62, an autophagy marker, were increased in induced isyn cells with Rab27b KD, whereas the early endosome marker Rab5 remained unchanged (Fig. 4). Similarly, LC3-positive puncta were increased in induced isyn cells with Rab27b KD under serum starvation compared with induced control isyn cells (Fig. 5*a*).

To further test the impact of Rab27b on autophagic flux, control isyn and isyn/Rab27b KD cells were induced with doxy for 96 h in serum-free medium followed by treatment with 40 μM chloroquine for 3 h. Chloroquine inhibits autophagosome/lysosome fusion, leading to an accumulation of LC3II in normal cells under autophagy-inducing conditions. Levels of LC3 II were increased in control isyn cells with chloroquine treatment, demonstrating an increase in autophagic flux (Fig. 5*b*). However, chloroquine failed to induce an increase in LC3 II in the presence of Rab27b KD in isyn cells (Fig. 5*b*). This finding points to a defect in autophagic flux with Rab27b KD. Partial colocalization of Rab27b with LC3

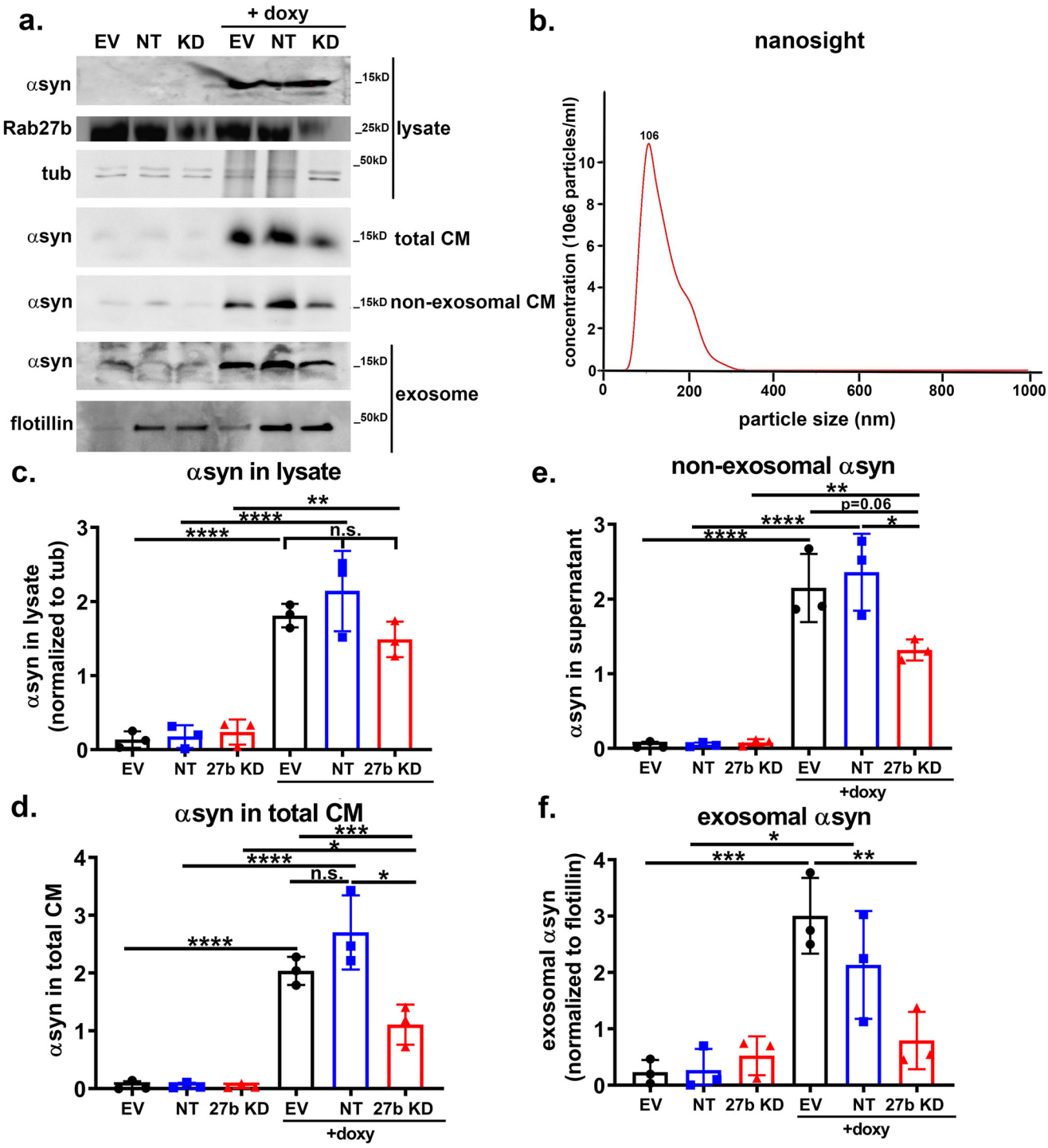

Figure 2. Rab27b knockdown reduces αsyn release into the CM. *a*, representative Western blots of total αsyn levels in CM and lysates from uninduced and induced isyn cell lines transduced with EV, nt-shRNA (*NT*), or Rab27b shRNA after doxy (10 μg/ml) induction for 96 h. Equal protein levels were loaded for each CM sample. *b*, NanoSight analysis shows that exosomal fraction from CM of control nt-shRNA–transduced isyn cells contains particles averaging 106 nm, consistent with the size of exosomes, after 96 h of induction with doxy. *c*, quantification of αsyn in the intracellular lysates from isyn cell lines transduced with EV, nt-shRNA, or Rab27b shRNA with and without 96-h induction by Western blotting. αsyn in lysates was normalized to tubulin. $n = 3$ independent rounds. One-way ANOVA: $F_{(5, 12)} = 34.43$, $p \leq 0.0001$. Sidak's multiple-comparison test: **, $p \leq 0.01$; ****, $p \leq 0.0001$. *n.s.*, nonsignificant. *d*, quantification of αsyn in total, unfractionated CM from isyn cell lines transduced with EV, nt-shRNA, or Rab27b shRNA with and without 96-h induction by Western blotting. Equal protein amounts were loaded for each CM sample. $n = 3$ independent rounds. One-way ANOVA: $F_{(5, 12)} = 40.21$, $p \leq 0.0001$. Sidak's multiple-comparison test: *, $p \leq 0.05$; ***, $p \leq 0.001$; ****, $p \leq 0.0001$; *n.s.*, nonsignificant. *e*, quantification of αsyn in the nonexosomal fraction from the CM from isyn cell lines transduced with EV, nt-shRNA, or Rab27b shRNA with and without 96-h induction by Western blotting. Equal protein amounts were loaded for each nonexosomal fraction sample. $n = 3$ independent rounds. One-way ANOVA: $F_{(5, 12)} = 43.13$, $p \leq 0.0001$. Sidak's multiple-comparison test: *, $p \leq 0.05$; ***, $p \leq 0.001$; ****, $p \leq 0.0001$. *f*, quantification of αsyn in the exosomal fraction from CM from isyn cell lines transduced with EV, nt-shRNA, or Rab27b shRNA with and without 96-h induction by Western blotting. Exosomal αsyn was normalized to flotillin. $n = 3$ independent rounds. One-way ANOVA: $F_{(5, 12)} = 12.20$, $p \leq 0.001$. Sidak's multiple-comparison test: *, $p \leq 0.05$; ***, $p \leq 0.001$; ***, $p \leq 0.001$. *Error bars*, S.D. *D*, doxy.

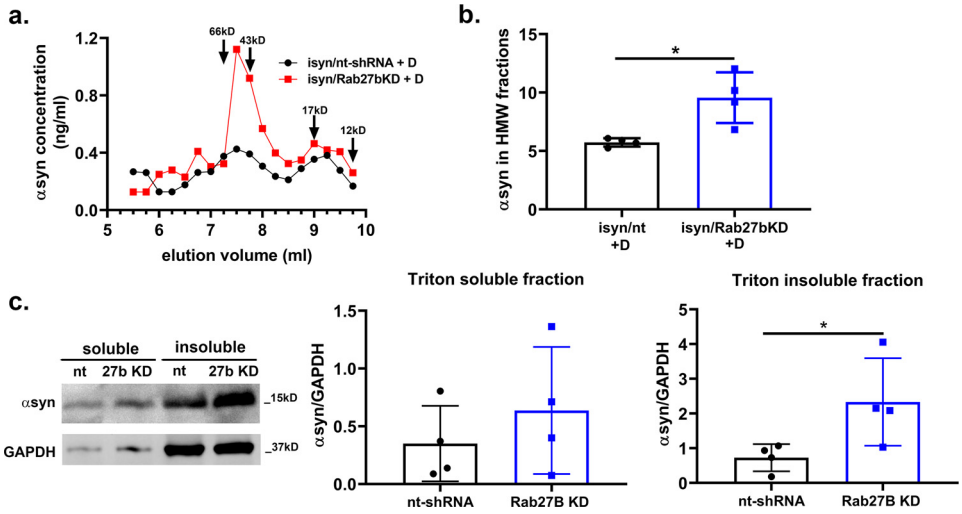

Figure 3. Rab27b knockdown increases release of higher-molecular-weight species of αsyn. *a*, αsyn levels in SEC fractions of CM from induced isyn/nt-shRNA cells or from induced isyn/Rab27b KD cells. Equal protein amounts (80 μg) per sample were loaded onto the column, and 250-μl fractions were collected from elution volume 4–12.5 ml. αsyn in each fraction was measured by ELISA. αsyn from CM from induced isyn/Rab27b cells was partially shifted into higher-molecular-weight fractions. Data are representative of four independent experiments. *b*, quantification of released αsyn detected in high-molecular-weight (*HMW*) SEC fractions collected between elution volumes 7.25 and 8.5 ml. $n = 4$ independent rounds. Student's *t* test: $t_6 = 3.484$; *, $p \leq 0.05$ (Student's *t* test). *c*, representative Western blotting and quantification of αsyn in Triton X-100–soluble and –insoluble fractions from induced isyn cell lines transduced with nt-shRNA (*nt*) or Rab27b shRNA after doxy (10 μg/ml) induction for 96 h. αsyn was normalized to glyceraldehyde-3-phosphate dehydrogenase (*GAPDH*). $n = 4$ independent rounds. Student's *t* test: $t_6 = 2.43$; *, $p \leq 0.05$ (Student's *t* test). *Error bars*, S.D. *D*, doxy.

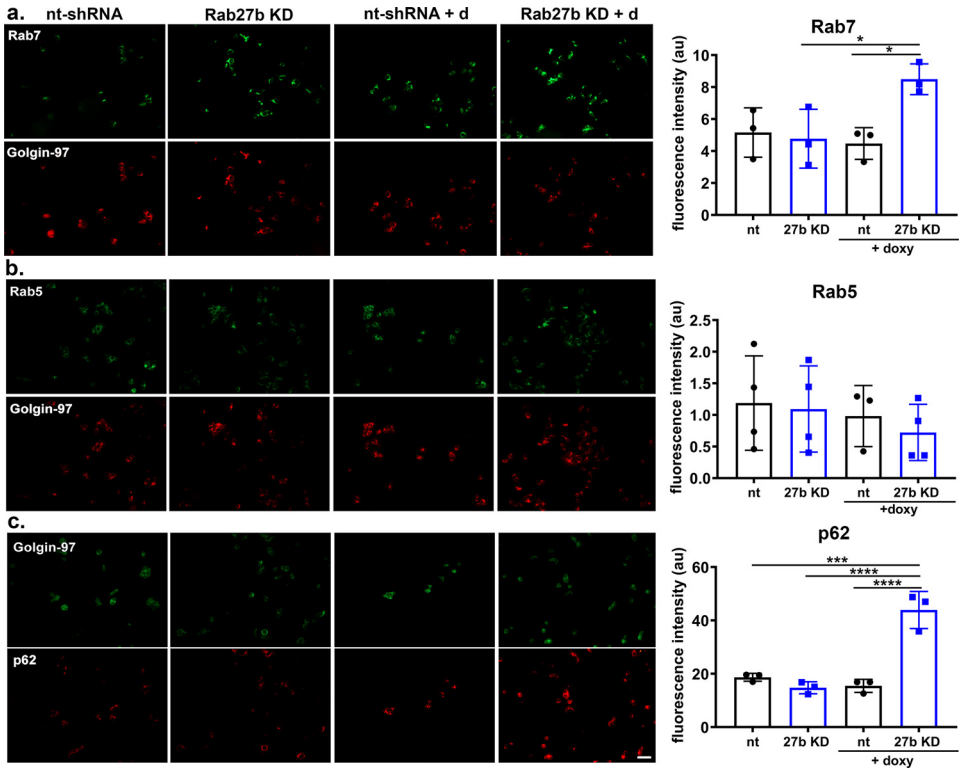

Figure 4. Rab27b knockdown increases Rab7 and p62 in isyn cells. *a*, representative images and quantification of Rab7, a late endosomal marker, in isyn cells with and without Rab27b KD when induced with doxy for 48 h. Rab7 fluorescence intensity is normalized to Golgin-97, a marker of early *trans*-Golgi network membranes. $n = 3$ independent rounds. One-way ANOVA: $F_{(3, 8)} = 5.443$, $p \leq 0.05$. Tukey's multiple-comparison test: *, $p \leq 0.05$. *b*, representative images and quantification of Rab5, an early endosomal marker, in isyn cells with and without Rab27b KD when induced with doxy for 48 h. Rab5 fluorescence intensity is normalized to Golgin-97. $n = 3$ independent rounds with 1–2 replicates/round. One-way ANOVA: $F_{(3, 11)} = 0.4304$, $p > 0.05$. *c*, representative images and quantification of p62 in isyn cells with and without Rab27b KD when induced with doxy for 48 h. p62 fluorescence intensity is normalized to Golgin-97. $n = 3$ independent rounds. One-way ANOVA: $F_{(3, 8)} = 37.57$, $p \leq 0.0001$. Tukey's multiple-comparison test: ***, $p \leq 0.001$; ****, $p \leq 0.0001$. *Error bars*, S.D. *D*, doxy. *Scale bar*, 50 μm.

and with LAMP1 in isyn cells demonstrates that Rab27b can interact with autophagosomes, lysosomes, and/or autolysosomes (Fig. 5, *c* and *d*). Together, these data suggest that Rab27b normally promotes autophagic αsyn clearance and that impaired autophagic clearance of αsyn by Rab27b KD promotes αsyn toxicity.

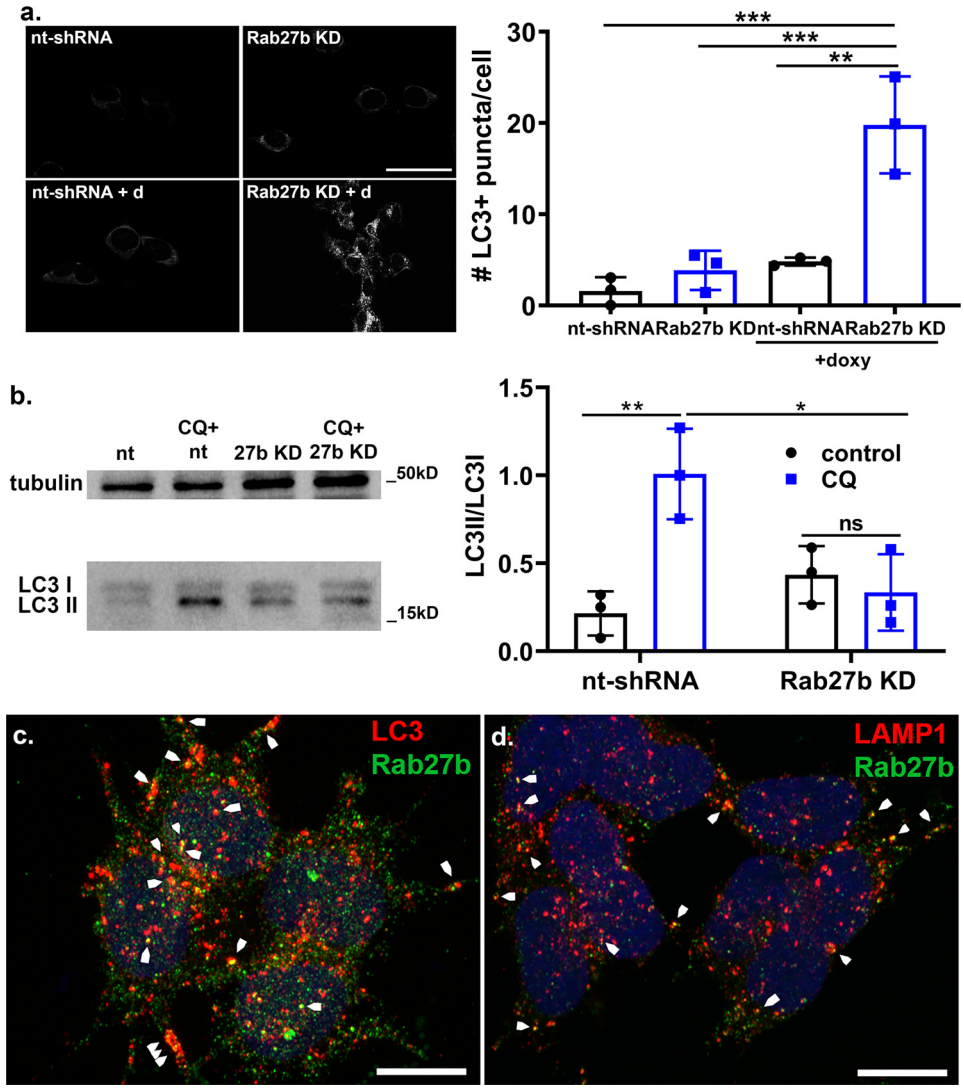

Figure 5. Rab27b knockdown reduces autophagic flux in isyn cells. *a*, Rab27b KD decreases LC3 puncta numbers compared with control. Representative images and quantification of LC3-positive puncta in isyn cells with and without Rab27b KD when induced with doxy for 48 h. *Scale bar*, 50 μm. $n = 3$ independent rounds, 17–36 cells quantified per group per round. One-way ANOVA: $F_{(3, 8)} = 23.32$, $p = 0.0003$. Tukey's multiple-comparison test: **, $p \leq 0.01$; ***, $p \leq 0.001$. *b*, Rab27b KD decreases LC3II accumulation when treated with the autophagosome-lysosome inhibitor chloroquine. Shown is representative Western blotting and quantification of LC3II/LC3I in isyn cells with and without Rab27b KD when induced with doxy for 48 h. $n = 3$ independent rounds. Two-way ANOVA: CQ treatment $F_{(1, 8)} = 9.206$, $p = 0.016$; cell line $F_{(1, 8)} = 3.946$, $p = 0.082$; interaction $F_{(1, 8)} = 15.29$, $p = 0.0045$. Tukey's multiple-comparison test: *, $p \leq 0.05$; **, $p \leq 0.01$; *ns*, nonsignificant. *c*, Rab27b partially colocalizes with LC3 in control isyn cells upon doxy induction. Shown is confocal image of LC3 (*red*) and Rab27b (*green*) immunoreactivity in induced isyn cells. *Arrowheads* point to colocalized punctae (*yellow*). *Scale bar*, 10 μm. *d*, Rab27b partially colocalizes with LAMP1 in control isyn cells upon doxy induction. Shown is a confocal image of LAMP1 (*red*) and Rab27b (*green*) immunoreactivity in induced isyn cells. *Arrowheads* point to colocalized punctae (*yellow*). *Scale bar*, 10 μm. *Error bars*, S.D. *D*, doxy.

Rab27b levels are increased in human PD and DLB

We evaluated Rab27b protein expression in the postmortem brain lysates in the medial temporal gyrus from age-matched controls and subjects with clinically and pathologically diagnosed PD or DLB. Rab27b levels were increased in the postmortem, Triton X-100 –soluble lysates of PD patients 2.1-fold compared with controls (Fig. 6*a*). Rab35 levels were not altered in PD brains compared with controls (Fig. 2*b*). Rab27b levels in the postmortem lysates of DLB patients were also increased by 20% compared with controls (Fig. 6*b*).

Discussion

Our data demonstrate that Rab27b regulates the release, clearance, and toxicity of αsyn in a cellular paracrine model. We observed that Rab27b KD in isyn cells increased αsyn paracrine toxicity. Rab27b KD induced a paradoxical decrease in αsyn release, but the lower levels of released αsyn were of higher-molecular-weight species. Rab27b KD also increased intracellular insoluble αsyn levels. We conclude that Rab27b KD leads to an increase in αsyn paracrine toxicity due to a reduction of clearance of misfolded αsyn through autophagy. Consistent with this, Rab27b KD led to increased LC3-positive autophagosome accumulation and p62 levels and inhibited autophagic flux. Together, these data suggest that Rab27b plays an integral role in the release, clearance, and toxicity of αsyn.

We have previously published on the advantages of our paracrine *in vitro* model that allows us to examine distinct parts of the various processes required for the prion-like spread of αsyn

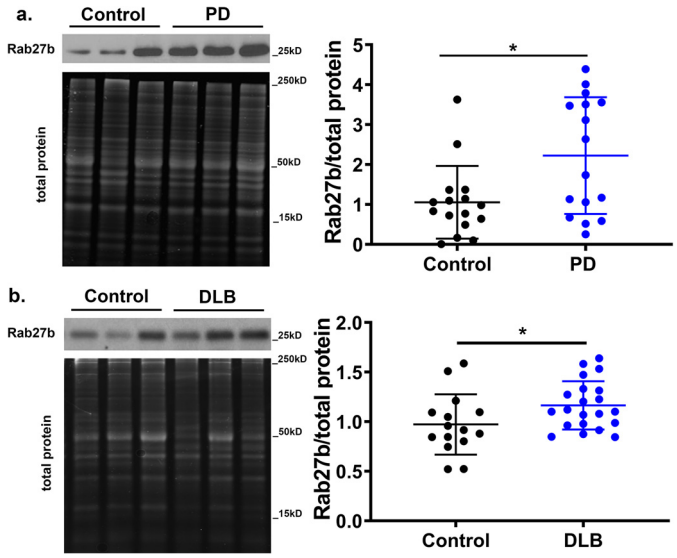

Figure 6. Rab27b protein expression is increased in human PD and DLB brains. *a*, representative Western blotting and quantification of Rab27b in control and PD postmortem temporal cortical lysates. Rab27b was normalized to total protein as determined by SYPRO Ruby Gel Protein Stain. $n = 16$ per group. Student's *t* test: $t_{30} = 2.716$; *, $p \leq 0.05$. *b*, representative Western blotting and quantification of Rab27b in control and PD postmortem temporal cortical lysates. Rab27b was normalized to total protein as determined by SYPRO Ruby Gel Protein Stain. $n = 15$ for control and $n = 21$ for DLB. Student's *t* test: $t_{34} = 2.113$; *, $p \leq 0.05$. *Error bars*, S.D.

(51). The studies detailed above indicate the potential cellular mechanisms by which Rab27b regulates αsyn spread and toxicity in this model. Our observations point to Rab27b as a regulator of αsyn propagation through multiple cellular mechanisms. Although Rab27b KD inhibited αsyn release, it also decreased autophagic flux, and released αsyn was more likely to promote toxicity. Despite the reduction in total amount of released αsyn, a probable shift to species capable of templating the misfolding of endogenous αsyn contributed to the increase in toxicity in cells treated with αsyn-enriched CM from isyn/Rab27b KD cells. Our previous studies have shown that the αsyn released into the CM is primarily oligomeric and promotes seeding (51). Given that insoluble αsyn was enhanced by Rab27b KD, our data suggest that the disruption of autophagy led to an increase in oligomeric, toxic αsyn release.

Together, these results indicate that Rab27b may function as an endogenous regulator of αsyn clearance via autophagy and release. Under normal conditions, we propose that Rab27b clears misfolded αsyn to prevent the intracellular buildup of toxic oligomers that can promote seeding by 1) promoting autophagic clearance and 2) promoting αsyn release (Fig. 7*a*). Disruption of Rab27b function allows for the accumulation of intracellular misfolded αsyn (Fig. 7*b*). Although total αsyn secretion is decreased by Rab27b depletion, any αsyn that is released has a higher seeding capacity and can then be taken up by neighboring neurons to induce pathologic seeding of endogenous αsyn (Fig. 7*b*). Rab27b depletion led to a decrease in αsyn release in both exosomal and nonexosomal fractions, indicating that multiple release mechanisms are regulated by Rab27b and may contribute to disease progression.

Rab27b levels were increased in the postmortem brain lysates of PD patients compared with age-matched healthy controls. We also found that Rab27b protein levels were increased in the brain lysates of DLB patients as well, in accordance with previously published transcriptome data (50). We propose that these increases in expression may be compensatory in nature. As intracellular misfolded protein accumulates, neurons may upregulate Rab27b to increase aggregated protein clearance through the autophagic pathway. Because Rab27b also promotes αsyn release, any increase in Rab27b in disease could theoretically promote αsyn transmission from cell to cell. However, as we have previously published, an increase in total amount of αsyn released into the CM does not necessarily correlate to increased paracrine toxicity but is instead dependent on the conformation of released αsyn (51). Indeed, our data show that Rab27b KD actually increased the toxicity of released αsyn despite lower total αsyn amounts in the CM; increased toxicity was likely due to the release of higher-molecular-weight species secondary to disrupted autophagic clearance.

The molecular mechanisms by which Rab27b regulates autophagic clearance and protein secretion are unclear at this time. Rab27b has been shown to promote distal transport and docking of secretory vesicles, including lysosomes, with the plasma membrane (28, 29, 31, 33, 36, 37, 41, 56, 58). Rab27b could potentially promote lysosomal fusion with the plasma membrane to promote αsyn secretion. Additionally, Rab27b could promote autophagic-lysosomal clearance of αsyn by promoting distal transport of lysosomes and fusion with autophagosomes. Consistent with this, the autophagic flux assay with the lysosomal inhibitor CQ (Fig. 5*b*) suggests that Rab27b does act at later stages in the autophagic-lysosomal pathway. Our data showing that Rab27b partially colocalizes with LAMP1 and LC3 point to its potential localization in autophagosomes, lysosomes, and/or fused autolysosomes (Fig. 5, *c* and *d*).

Rab effectors associated with Rab27b that are highly expressed in the brain include Slp5, Slp2a, rabphilin, Slac2a, and myrip (30), and we predict that different effectors are involved in the differential regulation of autophagic-lysosomal clearance *versus* secretion by Rab27b. Of these effectors, Slp5 (Sytl5) has been previously identified through shRNA screen by Goncalves *et al.* to regulate αsyn release (18). Other protein partners that may interact with Rab27b include motor proteins and SNARE proteins to promote vesicular transport and fusion. Motor proteins and adaptors are required partners for Rab proteins to aid transport (59, 60), and Rab27 isoforms have been shown to interact with kinesins to promote anterograde transport of secretory lysosomes and TrkB+ vesicles (38, 61). Once Rab27b has potentially brought lysosomes into position to fuse with the plasma membrane or autophagosomes, fusion would likely require tethering and SNARE proteins (59, 60).

Future directions will focus on these endolysosomal players that may interact with Rab27b, with a focus on the critical Rab27b effectors that regulate Rab27b's differential effects on autophagy and secretion. Testing the role of Rab27b in rodent or iPSC-based models of synucleinopathies will also be important in understanding the role of Rab27b in human disease. Whereas *in vitro* models are useful tools for testing basic cellular mechanisms, validation of these findings in more complex models is critical, given the limited biological complexity of cellular models.

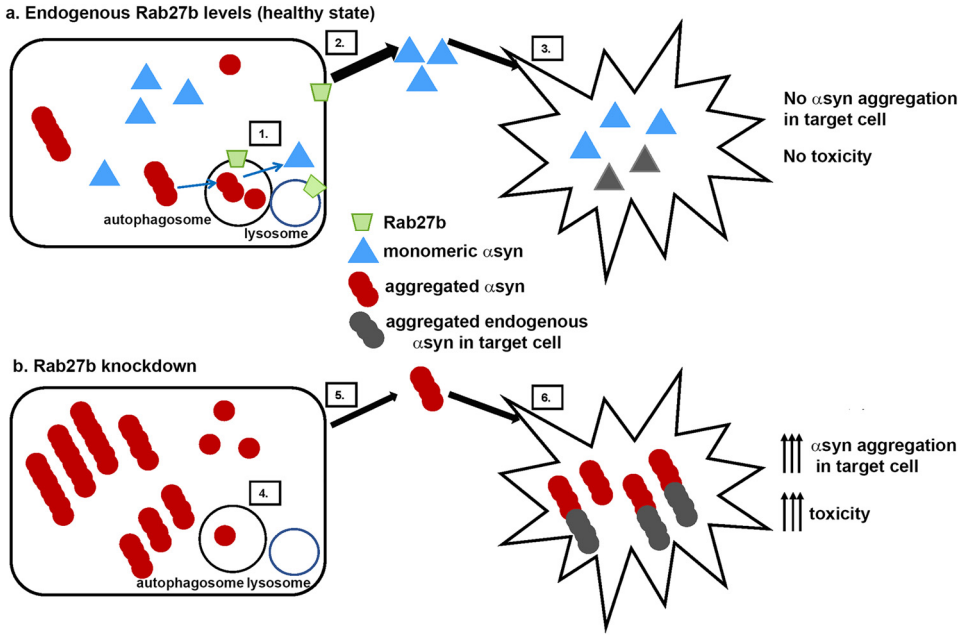

Figure 7. Model for Rab27b's effects on αsyn release and clearance. *a*, under normal circumstances, Rab27b decreases intracellular αsyn aggregation by increasing autophagic clearance of αsyn species (1). Rab27b also promotes the secretion of αsyn into the extracellular space (2), where the αsyn can be taken up by other neurons (3). *b*, upon Rab27b knockdown, intracellular αsyn aggregation increases by impaired autophagic clearance of αsyn (4). Whereas Rab27b KD decreases total αsyn release, the released αsyn has higher seeding potential (5), resulting in higher toxicity in neurons that take up the released αsyn (6).

In conclusion, Rab27b regulates αsyn toxicity in our paracrine model and is up-regulated in PD and DLB. Targeting Rab27b function could be a target for therapeutic intervention in these disorders.

Experimental procedures

Human brain samples

Human brain tissue was obtained from deceased persons, and the use of the human specimens was reviewed by the institutional review board at the University of Alabama at Birmingham and determined to be not human subjects research and not subject to Food and Drug Administration regulation. Sample identification was blinded and not available to the investigators. This work abides by the Declaration of Helsinki principles.

Cell lines

isyn cells were previously created by infecting SK-N-BE(2)-M17 (M17) male neuroblastoma cells (obtained and authenticated by ATCC (Manassas, VA), catalog no. CRL-2267; RRID:CVCL_0167) with the tetracycline-inducible αsyn pSLIK lentivirus in the presence of 6 μg/ml Polybrene followed by selection for stable transfection with G418 (62). isyn cells were maintained in 1:1 Eagle's MEM/F12K containing 10% fetal bovine serum (FBS), 1% penicillin/streptomycin, and G418 (500 μg/ml) at 37 °C. To induce αsyn expression, cells were treated with doxy at 10 μg/ml.

For Rab27b KD studies, isyn cells were transduced with a Rab27b-targeted shRNA (5′-CCCAAATTCATCACTACA-GTA-3′) (34), nontargeted shRNA (SHC016, Sigma–Aldrich), or empty vector plko.1 lentivirus, followed by selection for stable transfection with puromycin (1 μg/ml) in addition to G418 to maintain αsyn expression. Transduced cells were selected with 2 μg/ml puromycin 72 h later. Lines were maintained in 1:1 Eagle's MEM/F12K containing 10% FBS, 1% penicillin/streptomycin, G418 (500 μg/ml), and puromycin (1 μg/ml) at 37 °C. To induce αsyn expression, cells were treated with doxy at 10 μg/ml.

SH-SY5Y cells were obtained and authenticated by ATCC (catalog no. CRL-2266 RRID:CVCL_0019). SH-SY5Y cells were maintained in 1:1 Eagle's MEM/F12K containing 10% FBS and 1% penicillin/streptomycin. For differentiation, SH-SY5Y cells were treated with retinoic acid (10 μM) for 5–7 days in serum-free Eagle's MEM/F12K medium.

Preparation of CM

CM was prepared as described previously (51). After serial centrifugations to remove cellular debris, CM was concentrated using a 3-kDa Amicon Ultra-4 centrifugal filter at 4000 × *g* for 2 h, followed by dialysis. Protein concentrations of CM samples were assessed by BCA assay (Thermo Fisher Scientific), and equal protein amounts were loaded for each CM sample for Western blot analysis.

For toxicity experiments, isyn cells were induced with doxy in Eagle's MEM/F12K with 10% FBS for 1 week and then switched to serum-free Eagle's MEM/F12K for 48 h. Collected CM underwent centrifugation at 800 × *g* for 5 min and then at 2000 × *g* for 10 min and then at 10,000 × *g* for 30 min prior to transfer to differentiated SH-SY5Y cells.

Ethidium D cell death assay

Cells were rinsed in PBS and then incubated in 1 μM ethidium D and 2 μg/ml Hoechst 33342 in culture medium for 20 min at 37 °C. Ten high-power (×20) fields per well were randomly selected for quantification, and the number of ethidium D–positive cells and the total number of cells stained

Table 1
Primary antibodies used

Primary antibodies	Source	Identifier
Mouse monoclonal anti-α-synuclein	BD Biosciences	Catalog no. 610787 AB_398108
Rabbit polyclonal anti-α-synuclein	Cell Signaling Technology	Catalog no. 2642S AB_10695412
Mouse monoclonal anti-β-actin	Proteintech	Catalog no. 66009-lg AB_2687938
Mouse monoclonal anti-flotillin 1	BD Biosciences	Catalog no. 610820 AB_398139
Rabbit monoclonal anti-GAPDH	Cell Signaling Technology	Catalog no. 2118 AB_561053
Mouse monoclonal anti-Golgin97	Thermo Fisher Scientific	Catalog no. A-21270 AB_221447
Mouse monoclonal anti-LAMP-1	Developmental Studies Hybridoma Bank	Catalog no. H4A3 AB_2296838
Mouse monoclonal anti-LC3B	Abcam	Catalog no. ab243506
Rabbit polyclonal anti-LC3B	Cell Signaling Technology	Catalog no. 2775 AB_915950
Mouse monoclonal anti-p62	Abcam	Catalog no. ab56416 AB_945626
Rabbit monoclonal anti-Rab5	Abcam	Catalog no. ab109534 AB_10865740
Rabbit monoclonal anti-Rab7	Abcam	Catalog no. ab137029 AB_2629474
Mouse monoclonal anti-Rab27b	Proteintech	Catalog no. 66944–1-Ig
Mouse polyclonal anti-Rab27b	Abcam	Catalog no. ab76779 AB_1524280
Rabbit polyclonal anti-Rab27b	Millipore–Sigma	Catalog no. abs1026
Mouse monoclonal anti-α−tubulin	Sigma–Aldrich	Catalog no. T9026 AB_477593

by Hoechst 33342 were counted per high power field with the rater blind to experimental conditions.

Autophagic flux assay

isyn cells infected with nontargeted shRNA or Rab27b shRNA were induced with doxy at 10 μg/ml for 96 h in serum-free Eagle's MEM/F12K medium. Cells were then treated with vehicle or 40 μM chloroquine for 3 h at 37 °C prior to collection of cell lysates.

Western blotting

Western blot analysis was performed as described previously (51). Equal protein amounts were loaded per well for the CM samples and for cell lysate samples. Primary antibodies used are listed in Table 1. Blots were developed with the enhanced chemiluminescence method (GE Healthcare). Images were scanned using the Bio-Rad Chemidoc Imaging System and analyzed using Image Lab Bio-Rad software for densitometric analysis of bands.

Fresh-frozen tissue from temporal cortices of age and gender-matched control, PD, and DLB brains were obtained from the Banner Sun Health Research Institute Brain and Body Donation Program. Samples were prepared as described previously (57). Rab27b protein levels were normalized to total protein levels determined by SYPRO Ruby protein gel stain (Invitrogen).

Exosome fractionation

For exosome preparation, we followed the protocol described previously (51, 53). Briefly, cells were incubated to serum-free Eagle's MEM/F12K for 96 h. CM underwent serial centrifugations at 800 × *g* for 5 min, 2000 × *g* for 10 min, and 10,000 × *g* for 30 min to remove cellular debris at 4 °C. Debris-free medium was then spun at 100,000 × *g* for 2 h at 4 °C. The supernatant was saved as the nonexosomal fraction. The pellet was resuspended in PBS and then spun again at 100,000 × *g* for 80 min at 4 °C. The pellet was resuspended in PBS with protease inhibitors.

NanoSight

The size of exosomes was determined on a NanoSight NS300 (Malvern Instruments, Westboro, MA), as described previously (51). Following isolation by ultracentrifugation, exosome pellets were resuspended in 60 μl of cold PBS with repeated pipetting and vortexed for 10 s. Then 15 μl of the exosome suspension was diluted to a total volume of 1 ml of PBS and analyzed on a NanoSight NS300 infused with a syringe pump set at 25 (arbitrary units). Data were collected for each sample in 10 repeats of a 60-s video and analyzed using NanoSight NTA 3.0 software.

Size-exclusion chromatography

SEC was performed as described previously (51). 20 μl (80 μg) of CM diluted in PBS was loaded onto an NGC FPLC (Bio-Rad), injected on a Yarra 3-μm SEC-2000 column (300 × 7.8 mm; Phenomenex), and run at 0.7 ml/min in 1× PBS, pH 6.8. 250-μl fractions were collected from elution volume 4–12.5 ml. This corresponds to the end of the void volume, as determined by a blue dextran standard, and the buffer front, as determined by imidazole elution. αsyn in 50 μl of each fraction was measured using an ELISA for αsyn.

Immunocytochemistry

isyn cells were fixed in 4% paraformaldehyde for 15 min. After washing in PBS, cells were permeabilized with 0.5% Triton X-100 in PBS for 20 min and then blocked with 5% NGS in PBS for 20 min. Cells were incubated overnight with primary antibody (Rab27b, Rab5, Rab7, LC3II, p62, Golgin-97, LAMP1)

in 1.5% NGS. Primary antibodies used are described in Table 1. After washing, cells were incubated with goat anti-rabbit or anti-mouse secondary antibody in 1.5% NGS for 2 h. isyn cells were imaged using an Olympus BX51 epifluorescence microscope. Ten high-power (×20) fields per well were randomly selected for quantification, and the immunoreactivity was quantitated using ImageJ with the rater blind to experimental conditions. For LC3II puncta counts, slides were imaged at ×63 by confocal microscopy (Leica TCS-SP5 laser-scanning confocal microscope) and quantitated using an ImageJ cell counter. For Rab27b colocalization, Z-stack images of neurons were taken at ×63 by confocal microscopy (Nikon Eclipse Ti2 scanning confocal microscope).

Experimental design and statistical analysis

GraphPad Prism 8 (La Jolla, CA) was used for statistical analysis of experiments. Data were analyzed by either Student's *t* test or one-way or two-way ANOVA, followed by post hoc pairwise comparisons using Sidak's or Tukey's multiple-comparison tests. Statistical significance was set at $p \leq 0.05$. ANOVA-related statistics (F statistic, *p* values) and post hoc test results are found in the figure legends. For *t* tests, the *t* statistic and *p* values are noted in the figure legends.

Data availability

All data are contained in the article.

Acknowledgments—We are grateful to Drs. Geidy Serrano and Thomas Beach (Banner Sun Health Research Institute Brain and Body Donation Program, Sun City, AZ, USA) for the provision of human brain tissue. The Brain and Body Donation Program is supported by NIA, National Institutes of Health, Grant P30 AG19610 (Arizona Alzheimer's Disease Core Center); Arizona Department of Health Services Contract 211002 (Arizona Alzheimer's Research Center); Arizona Biomedical Research Commission Contracts 4001, 0011, 05-901, and 1001 to the Arizona Parkinson's Disease Consortium; and the Prescott Family Initiative of the Michael J. Fox Foundation for Parkinson's Research. Research reported in this publication was also supported by the University of Alabama Birmingham High Resolution Imaging Facility.

Author contributions—R. U. and T. A. Y. conceptualization; R. U., B. W., C. C., R. H. W., and T. A. Y. formal analysis; R. U., W. J. P., and T. A. Y. funding acquisition; R. U. and T. A. Y. validation; R. U., B. W., C. C., and R. H. W. investigation; R. U. and T. A. Y. visualization; R. U. and T. A. Y. methodology; R. U. and T. A. Y. writing-original draft; R. U., W. J. P., and T. A. Y. writing-review and editing; W. J. P. and T. A. Y. supervision; T. A. Y. resources; T. A. Y. project administration.

Funding and additional information—This study was supported by National Institutes of Health Grants R01 NS088533 (to T. A. Y.), R01 NS112203 (to T. A. Y.), P50 NS108675 (to T. A. Y.), R01GM117391 (to W. J. P.), and F31 NS106733 (to R. U.); the American Parkinson Disease Association; and the Parkinson Association of Alabama. The content is solely the responsibility of the authors and does not necessarily represent the official views of the National Institutes of Health.

Conflict of interest—The authors declare that they have no conflicts of interest with the contents of this article.

Abbreviations—The abbreviations used are: PD, Parkinson's disease; αsyn, α-synuclein; CM, conditioned medium; DLB, dementia with Lewy bodies; doxy, doxycycline; EV, empty vector; isyn, doxycycline-inducible α-synuclein cell line; KD, knockdown; nt-shRNA, nontarget shRNA; SEC, size-exclusion chromatography; MEM, minimal essential medium; FBS, fetal bovine serum; ANOVA, analysis of variance; NGS, normal goat serum.

References

1. Dorsey, E. R., Constantinescu, R., Thompson, J. P., Biglan, K. M., Holloway, R. G., Kieburtz, K., Marshall, F. J., Ravina, B. M., Schifitto, G., Siderowf, A., and Tanner, C. M. (2007) Projected number of people with Parkinson disease in the most populous nations, 2005 through 2030. *Neurology* **68,** 384–386 CrossRef Medline
2. Kordower, J. H., Chu, Y., Hauser, R. A., Freeman, T. B., and Olanow, C. W. (2008) Lewy body-like pathology in long-term embryonic nigral transplants in Parkinson's disease. *Nat. Med.* **14,** 504–506 CrossRef Medline
3. Danzer, K. M., Krebs, S. K., Wolff, M., Birk, G., and Hengerer, B. (2009) Seeding induced by α-synuclein oligomers provides evidence for spreading of α-synuclein pathology. *J. Neurochem.* **111,** 192–203 CrossRef Medline
4. Desplats, P., Lee, H. J., Bae, E. J., Patrick, C., Rockenstein, E., Crews, L., Spencer, B., Masliah, E., and Lee, S. J. (2009) Inclusion formation and neuronal cell death through neuron-to-neuron transmission of α-synuclein. *Proc. Natl. Acad. Sci. U.S.A.* **106,** 13010–13015 CrossRef Medline
5. Emmanouilidou, E., Melachroinou, K., Roumeliotis, T., Garbis, S. D., Ntzouni, M., Margaritis, L. H., Stefanis, L., and Vekrellis, K. (2010) Cell-produced α-synuclein is secreted in a calcium-dependent manner by exosomes and impacts neuronal survival. *J. Neurosci.* **30,** 6838–6851 CrossRef Medline
6. Lee, H. J., Patel, S., and Lee, S. J. (2005) Intravesicular localization and exocytosis of α-synuclein and its aggregates. *J. Neurosci.* **25,** 6016–6024 CrossRef Medline
7. Tsunemi, T., Perez-Rosello, T., Ishiguro, Y., Yoroisaka, A., Jeon, S., Hamada, K., Rammonhan, M., Wong, Y. C., Xie, Z., Akamatsu, W., Mazzulli, J. R., Surmeier, D. J., Hattori, N., and Krainc, D. (2019) Increased lysosomal exocytosis induced by lysosomal Ca^{2+} channel agonists protects human dopaminergic neurons from α-synuclein toxicity. *J. Neurosci.* **39,** 5760–5772 CrossRef Medline
8. Lee, H. J., Suk, J. E., Bae, E. J., Lee, J. H., Paik, S. R., and Lee, S. J. (2008) Assembly-dependent endocytosis and clearance of extracellular α-synuclein. *Int. J. Biochem. Cell Biol.* **40,** 1835–1849 CrossRef Medline
9. Liu, J., Zhang, J. P., Shi, M., Quinn, T., Bradner, J., Beyer, R., Chen, S., and Zhang, J. (2009) Rab11a and HSP90 regulate recycling of extracellular α-synuclein. *J. Neurosci.* **29,** 1480–1485 CrossRef Medline
10. Danzer, K. M., Kranich, L. R., Ruf, W. P., Cagsal-Getkin, O., Winslow, A. R., Zhu, L., Vanderburg, C. R., and McLean, P. J. (2012) Exosomal cell-to-cell transmission of alpha synuclein oligomers. *Mol. Neurodegener.* **7,** 42 CrossRef Medline
11. Ngolab, J., Trinh, I., Rockenstein, E., Mante, M., Florio, J., Trejo, M., Masliah, D., Adame, A., Masliah, E., and Rissman, R. A. (2017) Brain-derived exosomes from dementia with Lewy bodies propagate α-synuclein pathology. *Acta Neuropathol. Commun.* **5,** 46 CrossRef Medline
12. Lee, J.-G., Takahama, S., Zhang, G., Tomarev, S. I., and Ye, Y. (2016) Unconventional secretion of misfolded proteins promotes adaptation to proteasome dysfunction in mammalian cells. *Nat. Cell Biol.* **18,** 765–776 CrossRef Medline
13. Ejlerskov, P., Rasmussen, I., Nielsen, T. T., Bergström, A.-L., Tohyama, Y., Jensen, P. H., and Vilhardt, F. (2013) Tubulin polymerization-promoting protein (TPPP/p25α) promotes unconventional secretion of α-synuclein through exophagy by impairing autophagosome-lysosome fusion. *J. Biol. Chem.* **288,** 17313–17335 CrossRef Medline
14. Binotti, B., Jahn, R., and Chua, J. J. (2016) Functions of Rab proteins at presynaptic sites. *Cells* **5,** E7 CrossRef Medline
15. Lesage, S., Bras, J., Cormier-Dequaire, F., Condroyer, C., Nicolas, A., Darwent, L., Guerreiro, R., Majounie, E., Federoff, M., Heutink, P., Wood, N. W., Gasser, T., Hardy, J., Tison, F., Singleton, A., *et al.* (2015) Loss-of-

function mutations in *RAB39B* are associated with typical early-onset Parkinson disease. *Neurol. Genet.* **1,** e9 CrossRef Medline
16. Wilson, G. R., Sim, J. C., McLean, C., Giannandrea, M., Galea, C. A., Riseley, J. R., Stephenson, S. E., Fitzpatrick, E., Haas, S. A., Pope, K., Hogan, K. J., Gregg, R. G., Bromhead, C. J., Wargowski, D. S., Lawrence, C. H., *et al.* (2014) Mutations in RAB39B cause X-linked intellectual disability and early-onset Parkinson disease with α-synuclein pathology. *Am. J. Hum. Genet.* **95,** 729–735 CrossRef Medline
17. Gao, Y., Wilson, G. R., Stephenson, S. E. M., Bozaoglu, K., Farrer, M. J., and Lockhart, P. J. (2018) The emerging role of Rab GTPases in the pathogenesis of Parkinson's disease. *Mov. Disord.* **33,** 196–207 CrossRef Medline
18. Gonçalves, S. A., Macedo, D., Raquel, H., Simões, P. D., Giorgini, F., Ramalho, J. S., Barral, D. C., Ferreira Moita, L., and Outeiro, T. F. (2016) shRNA-based screen identifies endocytic recycling pathway components that act as genetic modifiers of α-synuclein aggregation, secretion and toxicity. *PLoS Genet.* **12,** e1005995 CrossRef Medline
19. Coune, P. G., Bensadoun, J. C., Aebischer, P., and Schneider, B. L. (2011) Rab1A over-expression prevents Golgi apparatus fragmentation and partially corrects motor deficits in an α-synuclein based rat model of Parkinson's disease. *J. Parkinsons Dis.* **1,** 373–387 CrossRef Medline
20. Dinter, E., Saridaki, T., Nippold, M., Plum, S., Diederichs, L., Komnig, D., Fensky, L., May, C., Marcus, K., Voigt, A., Schulz, J. B., and Falkenburger, B. H. (2016) Rab7 induces clearance of α-synuclein aggregates. *J. Neurochem.* **138,** 758–774 CrossRef Medline
21. Cooper, A. A., Gitler, A. D., Cashikar, A., Haynes, C. M., Hill, K. J., Bhullar, B., Liu, K., Xu, K., Strathearn, K. E., Liu, F., Cao, S., Caldwell, K. A., Caldwell, G. A., Marsischky, G., Kolodner, R. D., *et al.* (2006) α-Synuclein blocks ER-Golgi traffic and Rab1 rescues neuron loss in Parkinson's models. *Science* **313,** 324–328 CrossRef Medline
22. Dalfó, E., Barrachina, M., Rosa, J. L., Ambrosio, S., and Ferrer, I. (2004) Abnormal α-synuclein interactions with rab3a and rabphilin in diffuse Lewy body disease. *Neurobiol. Dis.* **16,** 92–97 CrossRef Medline
23. Yin, G., Lopes da Fonseca, T., Eisbach, S. E., Anduaga, A. M., Breda, C., Orcellet, M. L., Szegö;, É. M., Guerreiro, P., Lazaro, D. F., Braus, G. H., Fernandez, C. O., Griesinger, C., Becker, S., Goody, R. S., Itzen, A., *et al.* (2014) α-Synuclein interacts with the switch region of Rab8a in a Ser-129 phosphorylation-dependent manner. *Neurobiol. Dis.* **70,** 149–161 CrossRef Medline
24. Breda, C., Nugent, M. L., Estranero, J. G., Kyriacou, C. P., Outeiro, T. F., Steinert, J. R., and Giorgini, F. (2015) Rab11 modulates alpha-synuclein-mediated defects in synaptic transmission and behaviour. *Hum. Mol. Genet.* **24,** 1077–1091 CrossRef Medline
25. Alessi, D. R., and Sammler, E. (2018) LRRK2 kinase in Parkinson's disease. *Science* **360,** 36–37 CrossRef Medline
26. Chen, R. H., Wislet-Gendebien, S., Samuel, F., Visanji, N. P., Zhang, G., Marsilio, D., Langman, T., Fraser, P. E., and Tandon, A. (2013) α-Synuclein membrane association is regulated by the Rab3a recycling machinery and presynaptic activity. *J. Biol. Chem.* **288,** 7438–7449 CrossRef Medline
27. Mahoney, T. R., Liu, Q., Itoh, T., Luo, S., Hadwiger, G., Vincent, R., Wang, Z. W., Fukuda, M., and Nonet, M. L. (2006) Regulation of synaptic transmission by RAB-3 and RAB-27 in *Caenorhabditis elegans*. *Mol. Biol. Cell* **17,** 2617–2625 CrossRef Medline
28. Pavlos, N. J., Grønborg, M., Riedel, D., Chua, J. J., Boyken, J., Kloepper, T. H., Urlaub, H., Rizzoli, S. O., and Jahn, R. (2010) Quantitative analysis of synaptic vesicle Rabs uncovers distinct yet overlapping roles for Rab3a and Rab27b in Ca^{2+}-triggered exocytosis. *J. Neurosci.* **30,** 13441–13453 CrossRef Medline
29. Gomi, H., Mori, K., Itohara, S., and Izumi, T. (2007) Rab27b is expressed in a wide range of exocytic cells and involved in the delivery of secretory granules near the plasma membrane. *Mol. Biol. Cell* **18,** 4377–4386 CrossRef Medline
30. Fukuda, M. (2013) Rab27 effectors, pleiotropic regulators in secretory pathways. *Traffic* **14,** 949–963 CrossRef Medline
31. Shen, Y.-T., Gu, Y., Su W-F Zhong J-f Jin. Z-H, Gu, X.-S., and Chen, G. (2016) Rab27b is involved in lysosomal exocytosis and proteolipid protein trafficking in oligodendrocytes. *Neurosci. Bull.* **32,** 331–340 CrossRef Medline
32. Johnson, J. L., Brzezinska, A. A., Tolmachova, T., Munafo, D. B., Ellis, B. A., Seabra, M. C., Hong, H., and Catz, S. D. (2010) Rab27a and Rab27b regulate neutrophil azurophilic granule exocytosis and NADPH oxidase activity by independent mechanisms. *Traffic* **11,** 533–547 CrossRef Medline
33. Mizuno, K., Tolmachova, T., Ushakov, D. S., Romao, M., Abrink, M., Ferenczi, M. A., Raposo, G., and Seabra, M. C. (2007) Rab27b regulates mast cell granule dynamics and secretion. *Traffic* **8,** 883–892 CrossRef Medline
34. Ostrowski, M., Carmo, N. B., Krumeich, S., Fanget, I., Raposo, G., Savina, A., Moita, C. F., Schauer, K., Hume, A. N., Freitas, R. P., Goud, B., Benaroch, P., Hacohen, N., Fukuda, M., Desnos, C., *et al.* (2010) Rab27a and Rab27b control different steps of the exosome secretion pathway. *Nat. Cell Biol.* **12,** 19–30; sup pp 1–13 CrossRef Medline
35. Tolmachova, T., Abrink, M., Futter, C. E., Authi, K. S., and Seabra, M. C. (2007) Rab27b regulates number and secretion of platelet dense granules. *Proc. Natl. Acad. Sci. U.S.A.* **104,** 5872–5877 CrossRef Medline
36. Brozzi, F., Diraison, F., Lajus, S., Rajatileka, S., Philips, T., Regazzi, R., Fukuda, M., Verkade, P., Molnár, E., and Váradi, A. (2012) Molecular mechanism of myosin Va recruitment to dense core secretory granules. *Traffic* **13,** 54–69 CrossRef Medline
37. Handley, M. T., and Burgoyne, R. D. (2008) The Rab27 effector Rabphilin, unlike Granuphilin and Noc2, rapidly exchanges between secretory granules and cytosol in PC12 cells. *Biochem. Biophys. Res. Commun.* **373,** 275–281 CrossRef Medline
38. Arimura, N., Kimura, T., Nakamuta, S., Taya, S., Funahashi, Y., Hattori, A., Shimada, A., Ménager, C., Kawabata, S., Fujii, K., Iwamatsu, A., Segal, R. A., Fukuda, M., and Kaibuchi, K. (2009) Anterograde transport of TrkB in axons is mediated by direct interaction with Slp1 and Rab27. *Dev. Cell* **16,** 675–686 CrossRef Medline
39. Yi, Z., Yokota, H., Torii, S., Aoki, T., Hosaka, M., Zhao, S., Takata, K., Takeuchi, T., and Izumi, T. (2002) The Rab27a/granuphilin complex regulates the exocytosis of insulin-containing dense-core granules. *Mol. Cell. Biol.* **22,** 1858–1867 CrossRef Medline
40. Nozawa, T. (2018) [Selective autophagy mechanism against Group A Streptococcus infection]. *Nihon Saikingaku Zasshi* **73,** 193–199 CrossRef Medline
41. Chiang, L., Ngo, J., Schechter, J. E., Karvar, S., Tolmachova, T., Seabra, M. C., Hume, A. N., and Hamm-Alvarez, S. F. (2011) Rab27b regulates exocytosis of secretory vesicles in acinar epithelial cells from the lacrimal gland. *Am. J. Physiol. Cell Physiol.* **301,** C507–C521 CrossRef Medline
42. Pan, T., Kondo, S., Le, W., and Jankovic, J. (2008) The role of autophagy-lysosome pathway in neurodegeneration associated with Parkinson's disease. *Brain* **131,** 1969–1978 CrossRef Medline
43. Xilouri, M., Brekk, O. R., and Stefanis, L. (2016) Autophagy and α-synuclein: relevance to Parkinson's disease and related synucleopathies. *Mov. Disord.* **31,** 178–192 CrossRef Medline
44. Manzoni, C., and Lewis, P. A. (2013) Dysfunction of the autophagy/lysosomal degradation pathway is a shared feature of the genetic synucleinopathies. *FASEB J.* **27,** 3424–3429 CrossRef Medline
45. Chu, C. T. (2019) Mechanisms of selective autophagy and mitophagy: Implications for neurodegenerative diseases. *Neurobiol. Dis.* **122,** 23–34 CrossRef Medline
46. Vidyadhara, D. J., Lee, J. E., and Chandra, S. S. (2019) Role of the endolysosomal system in Parkinson's disease. *J. Neurochem.* **150,** 487–506 CrossRef Medline
47. Ginsberg, S. D., Mufson, E. J., Alldred, M. J., Counts, S. E., Wuu, J., Nixon, R. A., and Che, S. (2011) Upregulation of select rab GTPases in cholinergic basal forebrain neurons in mild cognitive impairment and Alzheimer's disease. *J. Chem. Neuroanat.* **42,** 102–110 CrossRef Medline
48. Lill, C. M., Abel, O., Bertram, L., and Al-Chalabi, A. (2011) Keeping up with genetic discoveries in amyotrophic lateral sclerosis: the ALSoD and ALSGene databases. *Amyotroph. Lateral Scler.* **12,** 238–249 CrossRef Medline
49. Herzfeld, T., Nolte, D., Grznarova, M., Hofmann, A., Schultze, J. L., and Müller, U. (2013) X-linked dystonia parkinsonism syndrome (XDP, lubag): disease-specific sequence change DSC3 in TAF1/DYT3 affects genes in vesicular transport and dopamine metabolism. *Hum. Mol. Genet.* **22,** 941–951 CrossRef Medline

50. Santpere, G., Garcia-Esparcia, P., Andres-Benito, P., Lorente-Galdos, B., Navarro, A., and Ferrer, I. (2018) Transcriptional network analysis in frontal cortex in Lewy body diseases with focus on dementia with Lewy bodies. *Brain Pathol.* **28,** 315–333 CrossRef Medline
51. Wang, B., Underwood, R., Kamath, A., Britain, C., McFerrin, M. B., McLean, P. J., Volpicelli-Daley, L. A., Whitaker, R. H., Placzek, W. J., Becker, K., Ma, J., and Yacoubian, T. A. (2018) 14–3-3 proteins reduce cell-to-cell transfer and propagation of pathogenic α-synuclein. *J. Neurosci.* **38,** 8211–8232 CrossRef Medline
52. Stuendl, A., Kunadt, M., Kruse, N., Bartels, C., Moebius, W., Danzer, K. M., Mollenhauer, B., and Schneider, A. (2016) Induction of α-synuclein aggregate formation by CSF exosomes from patients with Parkinson's disease and dementia with Lewy bodies. *Brain* **139,** 481–494 CrossRef Medline
53. Thery, C., Amigorena, S., Raposo, G., and Clayton, A. (2006) Isolation and characterization of exosomes from cell culture supernatants and biological fluids. *Curr. Protoc. Cell Biol.* Chapter 3, Unit 3.22 CrossRef Medline
54. Danzer, K. M., Ruf, W. P., Putcha, P., Joyner, D., Hashimoto, T., Glabe, C., Hyman, B. T., and McLean, P. J. (2011) Heat-shock protein 70 modulates toxic extracellular α-synuclein oligomers and rescues trans-synaptic toxicity. *FASEB J.* **25,** 326–336 CrossRef Medline
55. Malik, B. R., Maddison, D. C., Smith, G. A., and Peters, O. M. (2019) Autophagic and endo-lysosomal dysfunction in neurodegenerative disease. *Mol. Brain* **12,** 100 CrossRef Medline
56. Zhao, S., Torii, S., Yokota-Hashimoto, H., Takeuchi, T., and Izumi, T. (2002) Involvement of Rab27b in the regulated secretion of pituitary hormones. *Endocrinology* **143,** 1817–1824 CrossRef Medline
57. McFerrin, M. B., Chi, X., Cutter, G., and Yacoubian, T. A. (2017) Dysregulation of 14–3-3 proteins in neurodegenerative diseases with Lewy body or Alzheimer pathology. *Ann. Clin. Transl. Neurol.* **4,** 466–477 CrossRef Medline
58. Jaé, N., McEwan, D. G., Manavski, Y., Boon, R. A., and Dimmeler, S. (2015) Rab7a and Rab27b control secretion of endothelial microRNA through extracellular vesicles. *FEBS Lett.* **589,** 3182–3188 CrossRef Medline
59. Lorincz, P., and Juhasz, G. (2019) Autophagosome-lysosome fusion. *J. Mol. Biol.* **432,** 2462–2482 CrossRef Medline
60. Pu, J., Guardia, C. M., Keren-Kaplan, T., and Bonifacino, J. S. (2016) Mechanisms and functions of lysosome positioning. *J. Cell Sci.* **129,** 4329–4339 CrossRef Medline
61. Kurowska, M., Goudin, N., Nehme, N. T., Court, M., Garin, J., Fischer, A., de Saint Basile, G., and Ménasché, G. (2012) Terminal transport of lytic granules to the immune synapse is mediated by the kinesin-1/Slp3/Rab27a complex. *Blood* **119,** 3879–3889 CrossRef Medline
62. Slone, S. R., Lavalley, N., McFerrin, M., Wang, B., and Yacoubian, T. A. (2015) Increased 14-3-3 phosphorylation observed in Parkinson's disease reduces neuroprotective potential of 14-3-3 proteins. *Neurobiol. Dis.* **79,** 1–13 CrossRef Medline